



Visible light driven TaON/V₂O₅ heterojunction photocatalyst for deep elimination of volatile-aromatic compounds



Shaomang Wang^{a,b,c}, Zhongyu Li^b, Yuan Guan^b, Lei Lu^a, Zhan Shi^d, Peng Weng^b, Shicheng Yan^{a,*}, Zhigang Zou^{a,d}

^a Jiangsu Key Laboratory of Artificial Functional Materials, Eco-materials and Renewable Energy Research Center (ERERC), National Laboratory of Solid State Microstructures, Collaborative Innovation Center of Advanced Microstructures, College of Engineering and Applied Sciences, Nanjing University, No. 22 Hankou Road, Nanjing, Jiangsu 210093, PR China

^b School of Environment and Safety Engineering, Changzhou University, Changzhou, Jiangsu 213164, PR China

^c Changzhou University Huade College, Jingjiang, Jiangsu 214500, PR China

^d Jiangsu Province Key Laboratory for Nanotechnology, National Laboratory of Solid State Microstructures, School of Physics, Nanjing University, No 22 Hankou Road, Nanjing, Jiangsu 210093, PR China

ARTICLE INFO

Keywords:

Photocatalysis
Pollutant elimination
Volatile-aromatic compounds
TaON/V₂O₅ heterojunction

ABSTRACT

Efficiently separating carriers is the major challenge for degrading stable volatile-aromatic compounds by photocatalysis. Here, we propose using TaON to modify V₂O₅ to construct heterojunction for improving the charge separation efficiency. The 5 wt% TaON/V₂O₅ exhibited the optimal photocatalytic activity in degradation of toluene, reaching to 40% mineralization ratio after 30 h irradiation, which was 2.1 and 1.5 times higher than TaON and V₂O₅, respectively. The enhanced photocatalytic activity was mainly ascribed to the improved separation efficiency of carriers by the interface electric field of heterojunction. The mass spectrum and electron paramagnetic resonance analyses distinctly demonstrated that the toluene was first oxidized by OH to generate cyclohexane-1,2,3,4,5,6-hexaox. Then, it reacted with ·OH, ·O₂⁻ and h⁺ to change into xylose and methoxyacetaldehyde until they were mineralized to CO₂.

1. Introduction

Volatile aromatic compounds (VACs) are a class of volatile organic pollutants with benzene ring. Most VACs are a type of air pollutants of great concern due to their highly toxic and carcinogenic effect on humans [1–5]. Photocatalytic decomposition of VACs has caused wide concern because it is expected to utilize solar energy [6–8]. However, VACs are very stable and difficult to be photocatalytically degraded because of their molecular structure containing a big π bond. To destroy the big π bond of VACs, the photocatalyst must have high redox potential. UV-responsive photocatalysts usually meet this requirement. Thus, most photocatalysts for degradation of VACs were developed by modifying UV-responsive TiO₂ at present [9–13], while efficient photocatalysts with visible-light response for decomposition of VACs are lacking.

V₂O₅ has shown a certain potential as a visible-light-response catalyst with strong oxidation ability for decomposition of VACs owing to its band-gap energy of 2.1 eV and valence-band (VB) potential of 2.3 V (vs NHE) [14]. However, single V₂O₅ is low efficiency in removal of

VACs because of low separation efficiency of carriers. The construction of heterojunction is an effective way to improve separation efficiency of carriers. Researchers have developed some V₂O₅-based heterojunction photocatalysts such as V₂O₅/TiO₂ [15–18], V₂O₅/N-doped TiO₂ [19], V₂O₅/C-doped TiO₂ [20], V₂O₅/SmVO₄ [21], V₂O₅/MgF₂ [22], V₂O₅/YVO₄ [23], and V₂O₅/BiVO₄/TiO₂ [24] for degradation of VACs. However, in the above composite photocatalysts, V₂O₅ is only a visible-light-response sensitizer because of its small band gap. The V₂O₅ has rarely been reported as a primary catalyst in the heterogeneous photocatalysis for elimination of VACs. Herein, we dispersed the hundred-nanometer-size TaON nanoparticles onto surface of micrometer-size V₂O₅ bulk material to construct the visible-light-response TaON/V₂O₅ heterojunction [25–31]. A type-II heterojunction was built between TaON and V₂O₅ due to that the conduction-band (CB) potential of TaON is negative than CB of V₂O₅ and their valence band potentials are just on the contrary [14,32]. Therefore, charge separation was improved by the interface electric field of heterojunction. The 5 wt% TaON/V₂O₅ achieved efficient decomposition of typical VACs.

* Corresponding author.

E-mail address: yscfei@nju.edu.cn (S. Yan).

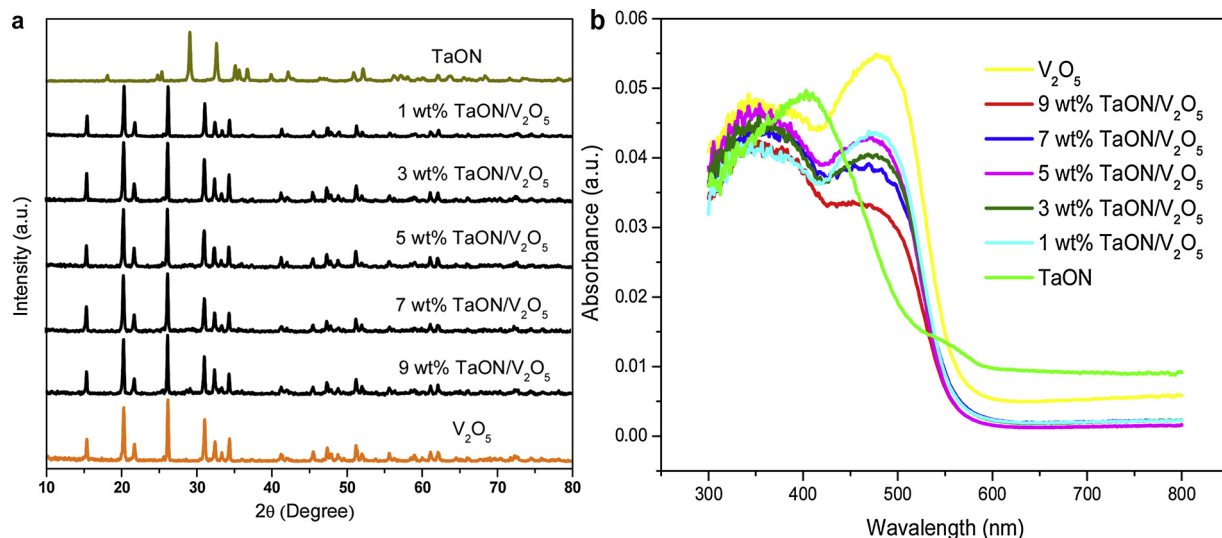


Fig. 1. (a) XRD patterns of TaON, V₂O₅, and TaON/V₂O₅ composites. (b) UV-vis absorption spectra of TaON, V₂O₅ and TaON/V₂O₅ composites.

2. Experimental section

2.1. Photocatalyst preparation

To synthesize TaON, typically, Ta₂O₅ powders (1.00 g) were uniformly dispersed on the bottom of an alumina crucible, and then calcined in a tube furnace (inner diameter 50 mm) at 850 °C for 10 h with a heating rate of 10 °C min⁻¹ under flowing NH₃ of 80 mL min⁻¹. The sample was naturally cooled to room temperature.

To obtain TaON/V₂O₅ composite photocatalysts, TaON (0.05 g) and NH₄VO₃ (1.22 g) were fully ground for 0.5 h with addition of 4 mL of ethanol. The mixture was dried at 100 °C for 1 h and then uniformly ground again. Subsequently, it was well-distributed on the bottom of an alumina crucible and calcined at 500 °C for 2.5 h with a heating rate of 5 °C min⁻¹. The 5 wt% TaON/V₂O₅ composite was obtained after naturally cooled to room temperature. The pure-phase V₂O₅ and other TaON/V₂O₅ composites with different content of TaON were prepared via the similar approach.

2.2. Characterization

The crystal structures of the samples were determined by powder X-ray diffraction (XRD) (Rigaku Ultima III, Japan) with Cu K α radiation ($\lambda = 1.5418 \text{ \AA}$). The scanning electron microscope (SEM) images were obtained via FEI NOVA Nano SEM 230. The elemental composition of the sample was analyzed by energy dispersive X-ray spectroscopy (EDX). Transmission electron microscope (TEM) images were collected from JEM-200CX. X-ray photoelectron spectroscopy (XPS) studies were performed on a PHI5000 Versa Probe (ULVAC-PHI, Japan) with monochromatized Al K α X-ray radiation (1486.6 eV). The UV-vis diffuse reflectance spectra (DRS) were recorded on a photospectrometer (UV-2550, Shimadzu). The BET surface area and pore diameter were measured by N₂ adsorption-desorption on an instrument (SA-3100, Beekman Coulter). Single-particle photoluminescence (PL) measurements were conducted on a FLS 980 spectrometer (Edinburgh Instruments, UK). A beam of laser with 488 nm generated by CW laser (Coherent, OBIS 488LS) excited the sample. The obtained data was further analyzed via the open software of ImagePro. Electron spin resonance (ESR) tests were performed on an apparatus (JES-FA200, JEOL). Photoelectrochemical measurements were conducted on an electrochemical analyzer (CHI-730E, Shanghai Chenhua, China) in a standard three-electrode system with a bias potential of 0.24 V vs. silver chloride electrode. Na₂SO₄ (1 mol L⁻¹) aqueous solution was utilized as the electrolyte. A platinum electrode and a silver chloride electrode

were used as counter electrode and reference electrode, respectively. Working electrode was prepared as follows: 40 mg of the sample and 10 mg of iodine were added to 50 mL of acetone with ultrasonic shock for half an hour. Then, the sample was deposited on a fluorine-doped tin oxide conducting substrate with a fixed area of 1 cm² by a voltage of 15 V for 3 min. A 300 W Xe lamp was used as the light source for photocurrent measurement.

2.3. Calculation method

The function of b3lyp was used to calculate molecular energy. The basis set was 6-31g and the convergence criteria was tight. The d-polarized orbit and p-polarized orbit were added to non-hydrogen atoms and hydrogen atoms, respectively.

2.4. Evaluation of photocatalytic activity

The photocatalytic reactions were conducted in a gas sealed container with a volume of 250 mL. The as-prepared photocatalyst (0.2 g) was uniformly dispersed on the bottom of the reaction container. Toluene gas with 50 μL of H₂O was injected into the reactor such that the initial concentration of toluene in the reactor was 3000 ppm. The system was kept in the dark for 1 h to ensure that the adsorption-desorption equilibrium was established. A 300 W Xenon arc lamp was used as light source. During the irradiation, 100 μL of gas withdrawn from the above system every two hours was analyzed by a gas chromatograph (GC9790, Fuli).

3. Results and discussion

3.1. Characterization of photocatalysts

The crystal structures of the photocatalysts are shown in Fig. 1a. The XRD peaks of the sample prepared by nitriding Ta₂O₅ were consistent with monoclinic structure of TaON (JCPDS card no. 70-1193) [33]. The diffraction peaks of V₂O₅ could be clearly indexed as orthorhombic structure (JCPDS card no. 72-0598). The V₂O₅ was loaded on the TaON by a simple heat treatment of fully mixed TaON and NH₄VO₃ at 500 °C. The diffraction peaks of TaON/V₂O₅ composites were similar to those of V₂O₅. The diffraction peaks of TaON were not found in the TaON/V₂O₅ composites with low content of TaON. With the increase of TaON content, the characteristic diffraction peak of TaON at about 28° was observed. In addition, the diffraction peak at 32.5° in the 1 wt% TaON/V₂O₅ composites was slightly forked compared to that of V₂O₅. As the

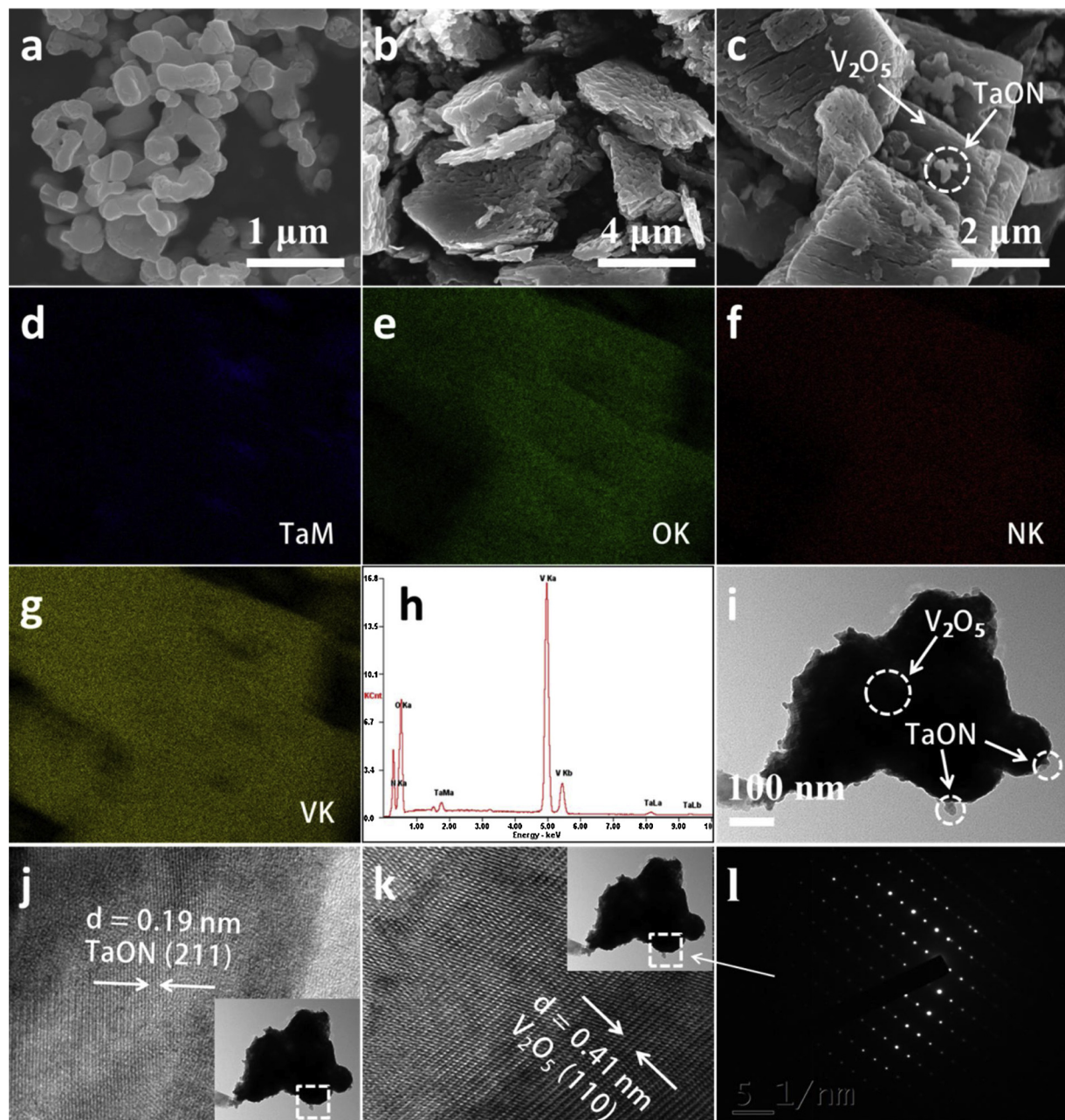


Fig. 2. SEM images of (a) TaON, (b) V₂O₅ and (c) 5 wt% TaON/V₂O₅. Element mapping of (d) Ta, (e) O, (f) N and (g) V, and (h) EDX for (c) 5 wt% TaON/V₂O₅. TEM images of (i, j, k and l) 5 wt% TaON/V₂O₅.

content of TaON increased, the peak was more distinctly forked. It is basically caused by the interaction between (011) crystal facet of V₂O₅ and (111) crystal plane of TaON. The results confirm that during the heat treatment, the NH₄VO₃ is decomposed and is oxidized to V₂O₅, and hence forming TaON/V₂O₅ composite.

The optical properties of TaON, V₂O₅ and TaON/V₂O₅ composites are depicted in Fig. 1b. The maximum absorption wavelength of TaON was about 550 nm with the band-gap energy of 2.3 eV. The V₂O₅ could absorb solar energy with a wavelength shorter than 578 nm, and its band-gap energy was approximately 2.1 eV. With the increase of TaON content, the absorbance edge of TaON/V₂O₅ composites showed a gradual blue shift, but they exhibited the slight difference in the range of 570–572 nm. The results imply that the TaON/V₂O₅ composites possess good absorption of visible light.

As depicted in Fig. 2, TaON with particle diameter of about 100–250 nm displayed pebble shape (Fig. 2a). V₂O₅ exhibited bulk

appearance and its particle size was about 2–6 μm (Fig. 2b). Two particle shapes were also observed in the 5 wt% TaON/V₂O₅. Small pebble particle was TaON and big bulk particle was V₂O₅ (Fig. 2c). In addition, it is expressly seen that the TaON nanoparticles anchored the surface of V₂O₅ and were well dispersed. The element mapping and EDX confirmed that the 5 wt% TaON/V₂O₅ contained four elements of Ta, N, O, and V (Fig. 2d–h). TEM illustrated that TaON and V₂O₅ contacted tightly (Fig. 2i). The lattice spacing of 0.19 and 0.41 nm corresponded to (211) crystal plane of TaON and (110) crystal face of V₂O₅, respectively, which further reveals that the mixture of TaON and NH₄VO₃ calcined at 500 °C for 2.5 h change to the hybrid materials of TaON and V₂O₅. Selected area electron diffraction on the particle interface demonstrated that both TaON and V₂O₅ nanoparticles were single crystal (Fig. 2j–l). These results indicate that the high-quality interface between TaON and V₂O₅ can be formed by a simple heat treatment that is easy to industrial applications.

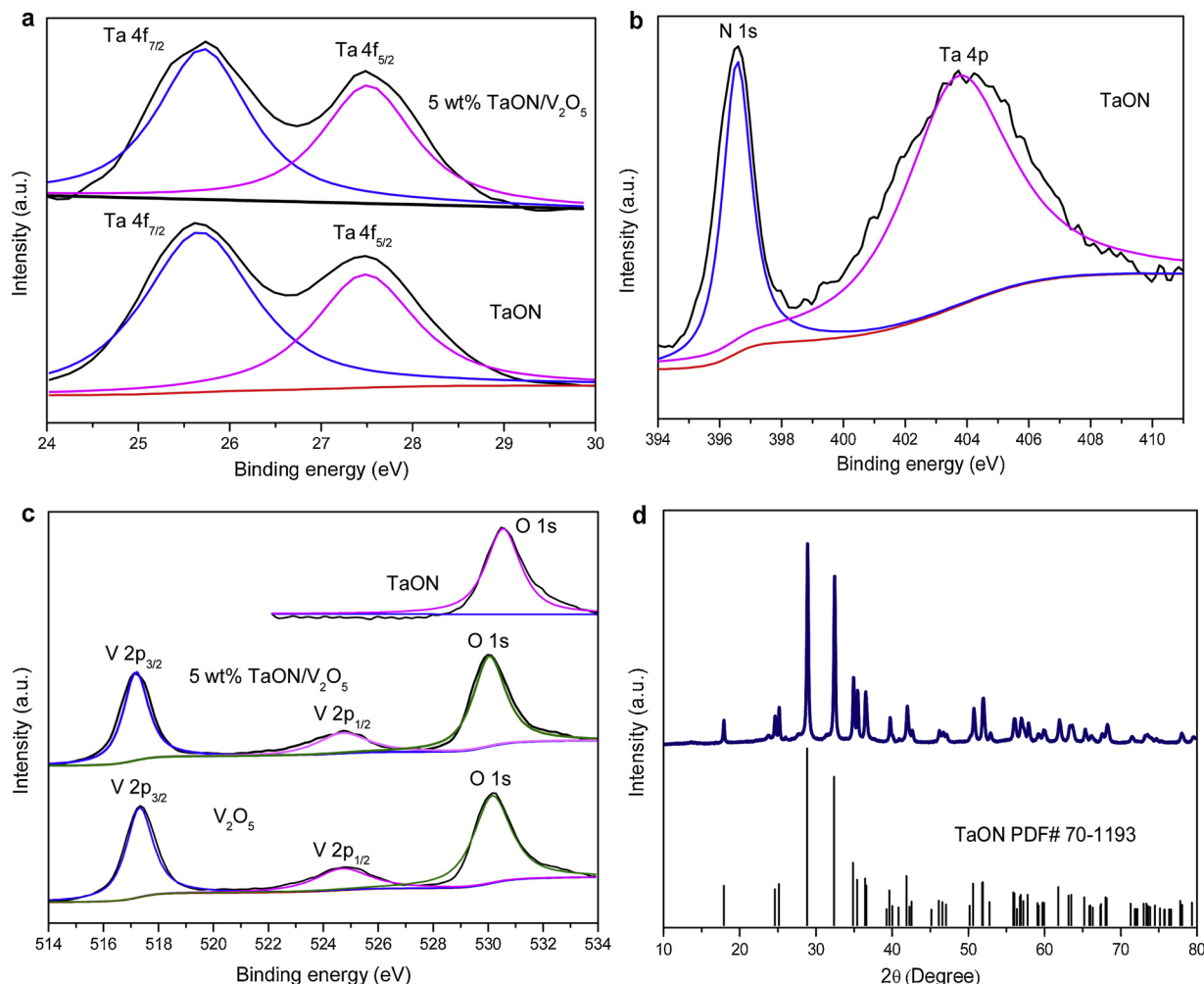


Fig. 3. XPS core-level spectra of (a) Ta 4f, (b) N 1s and Ta 4p, (c) V 2p and O 1s. XRD pattern of (d) TaON after calcining at 500 °C for 2.5 h in air.

The chemical composition and elemental valence in the surface of as-fabricated photocatalysts are shown in Fig. 3. Three elements, Ta, O, and N, were detected (Fig. 3a–c), which are consistent with the chemical composition of TaON. Only three elements of Ta, O and V were identified in the 5 wt% TaON/V₂O₅. The XRD pattern of TaON calcined at 500 °C for 2.5 h was in accord with its monoclinic structure (Fig. 3d). Thus, in our case of preparation of TaON/V₂O₅, it is believed that the TaON is stable during heat treatment. The binding energies of Ta 4f_{7/2} and Ta 4f_{5/2} in the 5 wt% TaON/V₂O₅ and TaON respectively were 25.7 and 27.5 eV [33], which correspond to Ta⁵⁺. The peak at 403.7 eV in the TaON originates from Ta 4p_{3/2} [34]. The peak of N 1s at 396.7 eV in the TaON belongs to N⁻³. The binding energies of V 2p_{3/2} and V 2p_{1/2} were 517.3 and 524.7 eV in the 5 wt% TaON/V₂O₅ and V₂O₅ [35], which belong to V⁵⁺. The binding energies of O 1s belonging to O²⁻ exhibited the order of 5 wt% TaON/V₂O₅ (530.1 eV) < V₂O₅ (530.2 eV) < TaON (530.5 eV). It is caused by different coordination environment of surface lattice oxygen. The results further confirm that the TaON/V₂O₅ composites are successfully synthesized. The slight decrease in O1 s binding energy of TaON/V₂O₅ may indicate a strong interaction between TaON and V₂O₅, which induces the electron transfer at their interface.

3.2. Photocatalytic performances of photocatalysts

The experiments of toluene removal over as-prepared photocatalysts were performed for 30 h irradiation after the dark adsorption for 1 h, and the results are displayed in Fig. 4. Under the dark condition,

the initial toluene concentration dropped from 3000 ppm to 2157, 1675, 2051, 1935, 1799, 1958 and 1847 ppm over TaON, V₂O₅, and 1–9 wt% TaON/V₂O₅, respectively. The concentration of CO₂ was not increased and kept the initial about 350 ppm in the system. It means that the toluene is able to adsorb on as-prepared photocatalysts. Under 2 h irradiation, the toluene concentration slightly increased over TaON, V₂O₅, 3 wt% TaON/V₂O₅, and 9 wt% TaON/V₂O₅, while that continued to decrease over 1 wt% TaON/V₂O₅, 5 wt% TaON/V₂O₅, and 7 wt% TaON/V₂O₅. The concentration of CO₂ increased in each reaction system. This indicates that the desorption rate of toluene is faster than its decomposition rate over TaON, V₂O₅, 3 wt% TaON/V₂O₅, and 9 wt% TaON/V₂O₅, while the desorption rate of toluene is slower than its decomposition rate over 1 wt% TaON/V₂O₅, 5 wt% TaON/V₂O₅, and 7 wt% TaON/V₂O₅. After 30 h irradiation, the concentration of toluene was 890, 600, 283, 500, 120, 294, and 503 ppm, and the concentration of CO₂ was 1333, 1779, 2090, 1896, 2298, 2167, and 1979 ppm over TaON, V₂O₅ and 1–9 wt% TaON/V₂O₅, respectively. The 5 wt% TaON/V₂O₅ exhibited the optimal photocatalytic activity. The degradation ratio of toluene was about 93% over 5 wt% TaON/V₂O₅, which was 1.6 and 1.4 times as high as that over TaON and V₂O₅, respectively. The mineralization ratio of toluene was approximately 40% over 5 wt% TaON/V₂O₅, which was 2.1 and 1.5 as high as that over TaON and V₂O₅, respectively. The toluene degradation by reusing the 5 wt% TaON/V₂O₅ for four reaction cycles showed that the degradation rate of toluene and CO₂ generation did not decrease markedly. No obvious changes in XRD patterns of 5 wt% TaON/V₂O₅ before and after the reaction were observed. These facts display that the 5 wt% TaON/V₂O₅

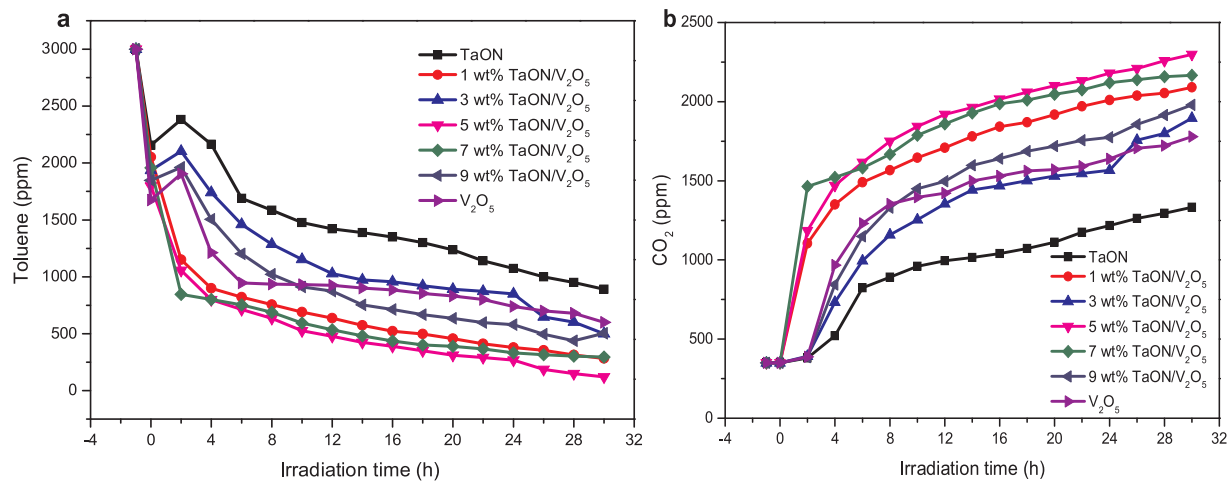


Fig. 4. (a) The concentration change of toluene over TaON, V₂O₅, and TaON/V₂O₅ composites with irradiation time. (b) The concentration change of CO₂ over TaON, V₂O₅, and TaON/V₂O₅ composites with irradiation time.

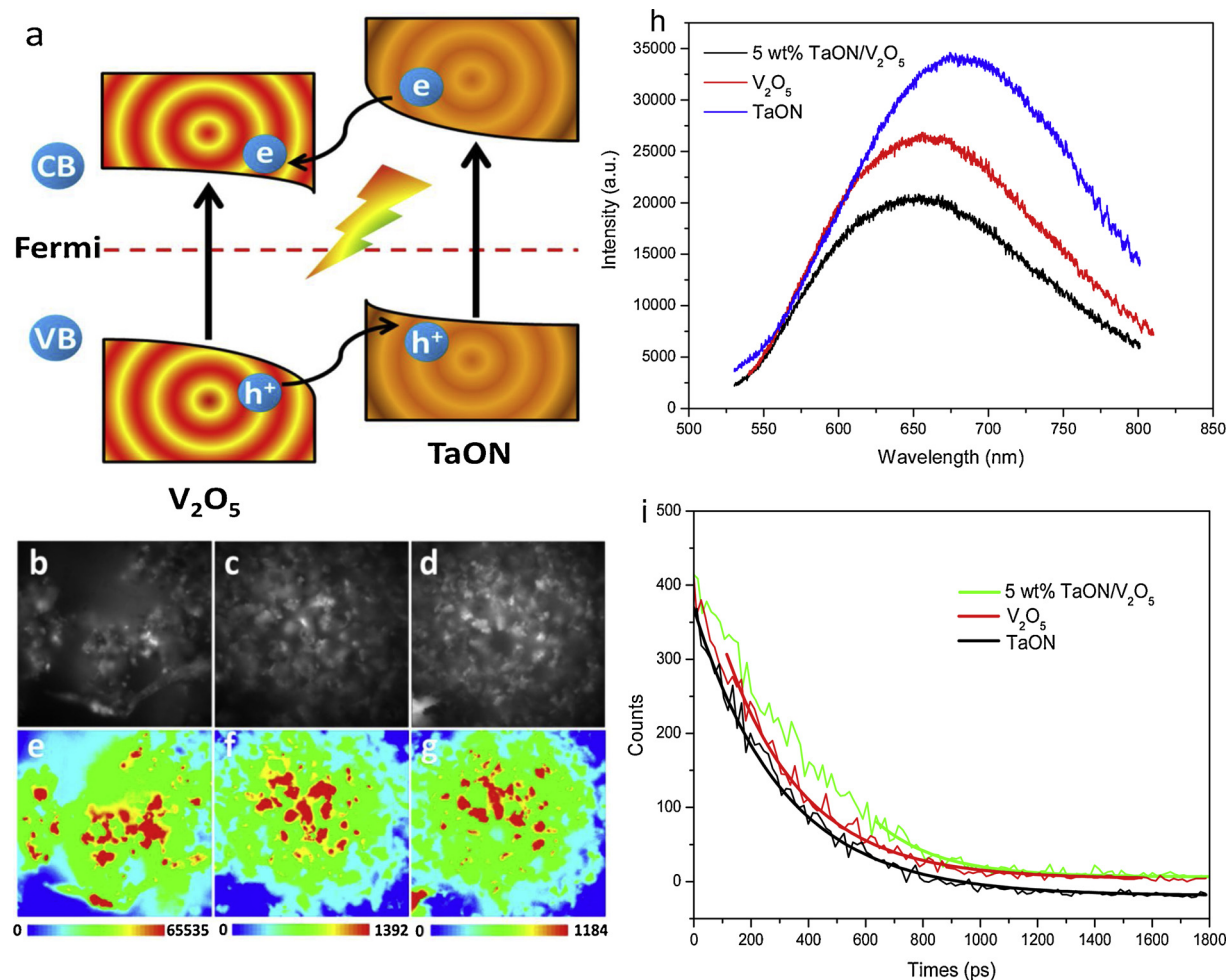


Fig. 5. (a) Schematic illustration of electron-hole separation at the interface of TaON/V₂O₅ junction. Fluorescence images of (b and e) TaON, (c and f) V₂O₅ and (d and g) 5 wt% TaON/V₂O₅. (h) Single-particle fluorescence spectroscopy of TaON, V₂O₅ and 5 wt% TaON/V₂O₅. (i) Fluorescence decay profile of TaON, V₂O₅ and 5 wt% TaON/V₂O₅.

has good stability (Figs. S1 and 2).

3.3. Mechanisms of the enhanced photocatalytic activity

Generally, the photocatalysts with large specific surface area and

pore size can provide more active sites for the photocatalytic degradation of pollutants. The specific surface area and average pore diameter were $4.3 \text{ cm}^2 \text{ g}^{-1}$ and 32 nm for TaON, $5.8 \text{ cm}^2 \text{ g}^{-1}$ and 38 nm for V₂O₅, and $6.9 \text{ cm}^2 \text{ g}^{-1}$ and 37.6 nm for 5 wt% TaON/V₂O₅ (Fig. S3). Compared to TaON and V₂O₅, 5 wt% TaON/V₂O₅ with the

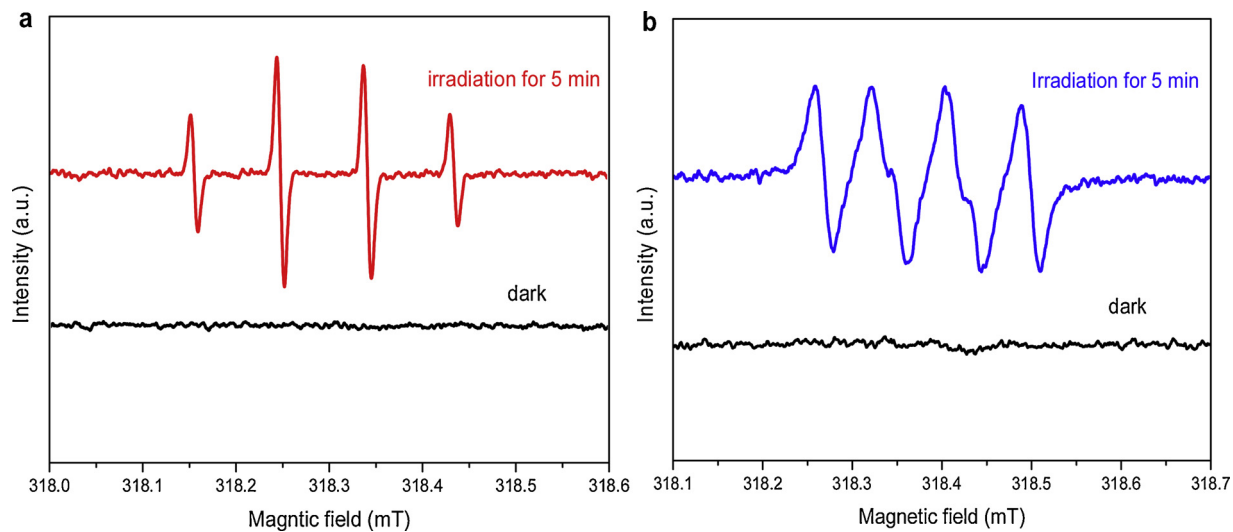


Fig. 6. ESR spectra of 5 wt% TaON/V₂O₅ using DMPO as a radical scavenger under aqueous solution (a) and methanol solution (b).

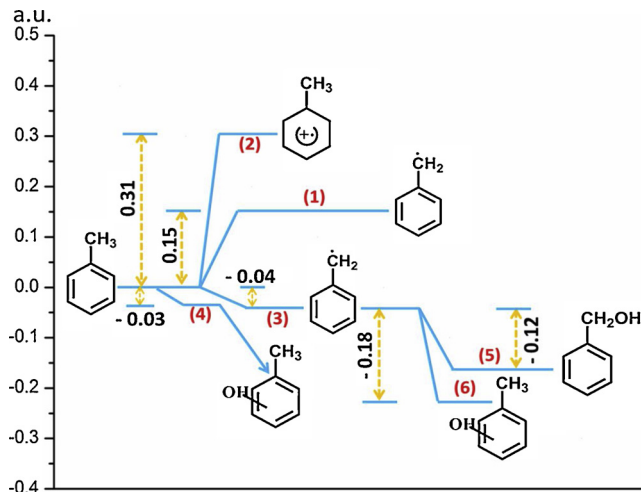


Fig. 7. The calculated energy requirement for the oxidation of toluene.

larger specific surface area can stably adsorb more toluene, which promotes the photocatalytic degradation of toluene. If a photocatalyst can generate much effective photoinduced electrons and holes, it can efficiently degrade pollutants by producing much catalytically active species. Under light excitation of TaON/V₂O₅ composites, electrons from the conduction band (CB) of TaON will migrate to CB of V₂O₅, and holes from the valence band (VB) of V₂O₅ will diffuse to VB of TaON according to the potential difference of V₂O₅ ($E_{CB} = 0.2$ and $E_{VB} = 2.3$ V) [14] and TaON ($E_{CB} = -0.3$ and $E_{VB} = 2.1$ V) [32] (Fig. 5a). This greatly promotes separation of photogenerated electron-hole pairs of TaON/V₂O₅ composites, thereby significantly enhancing its photocatalytic activity.

Single-particle fluorescence spectroscopy was used to characterize separation efficiency of carriers of TaON, V₂O₅, and 5 wt% TaON/V₂O₅. As depicted in Fig. 5b-h, the strong red fluorescence was observed from TaON showing a strong signal of emission peak at about 675 nm. V₂O₅ emitted weaker red fluorescence with lower intensity of emission spectrum at approximately 655 nm. It can be clearly seen that 5 wt% TaON/V₂O₅ exhibited weakest red fluorescence with further decreasing peak intensity at about 655 nm. Therefore, compared to TaON and V₂O₅, separation efficiency of carriers of 5 wt% TaON/V₂O₅ is significantly improved, which greatly enhances its photocatalytic activity. Fluorescence lifetime and photocurrent were utilized to further analyze separation efficiency of carriers of TaON, V₂O₅, and 5 wt% TaON/V₂O₅.

As shown in Figs. 5i and S4, the fluorescence lifetime and photocurrent were exhibited the order of 5 wt% TaON/V₂O₅ > V₂O₅ > TaON, confirming the highest charge separation efficiency of 5 wt% TaON/V₂O₅, in good consistent with PL results.

3.4. Photocatalytic decomposition mechanism of toluene

As we all know, free radicals such as ·OH and ·O₂⁻ are basically active species except photogenerated electrons and holes in photocatalytic degradation reaction. ESR technique was utilized to determine radical generated over 5 wt% TaON/V₂O₅ using DMPO as a radical scavenger under light irradiation. As illustrated in Fig. 6, no signal was observed under the dark. Four peaks with the signal intensity of 1:2:2:1 appeared at H₂O solution under irradiation for 5 min, which is a typical ESR signal of ·OH. There were four peaks with the signal intensity of 1:1:1:1 found at methanol solution under irradiation for 5 min, corresponding to the ESR signal of ·O₂⁻. ESR results demonstrate that main radicals for the photocatalytic degradation of toluene over 5 wt% TaON/V₂O₅ are ·OH and ·O₂⁻.

The Sleiman et al. have proposed reaction pathway for the photocatalytic degradation of toluene, which is shown in Fig. S5. According to the proposed pathway, we further explore the photocatalytic degradation pathway of toluene by theoretical calculations. A possible route is that toluene is oxidized to generate benzyl radical and positive ion of toluene by the hole, requiring to absorb 0.15 and 0.31 a.u. of energy, respectively. Another possible route is that toluene is oxidized to produce benzyl radical and hydroxytoluene by hydroxyl radical, releasing 0.04 and 0.03 a.u., respectively. Thus, as shown in Fig. 7, the toluene degradation tends to follow route 1 and route 3 under anhydrous condition and in the presence of water, respectively. Benzyl radical is oxidized to generate benzyl alcohol and hydroxytoluene by hydroxyl radical, companying energy release of 0.12 and 0.18 a.u., respectively. Therefore, Benzyl radical further oxidized tends to follow route 6. Hydroxytoluene is further oxidized to produce hydroxyphenol tending to follow route 7. Then, its ring is opened to generate CO₂ and H₂O. The intermediates of toluene degradation were identified by GC-MS. Only toluene was determined via fragment ion of *m/z* = 92, 91, and 44 during the dark adsorption (Fig. S9). The detection of intermediate is very important for understanding the reaction mechanism of a given photocatalytic reaction. However, it is difficult to detect the all intermediates due to the their fast reaction kinetics. In this study, two important intermediates, xylose and methoxyacetaldehyde, were identified by GC-MS. The xylose and methoxyacetaldehyde, as relatively stable intermediates in the final reaction steps for degradation of

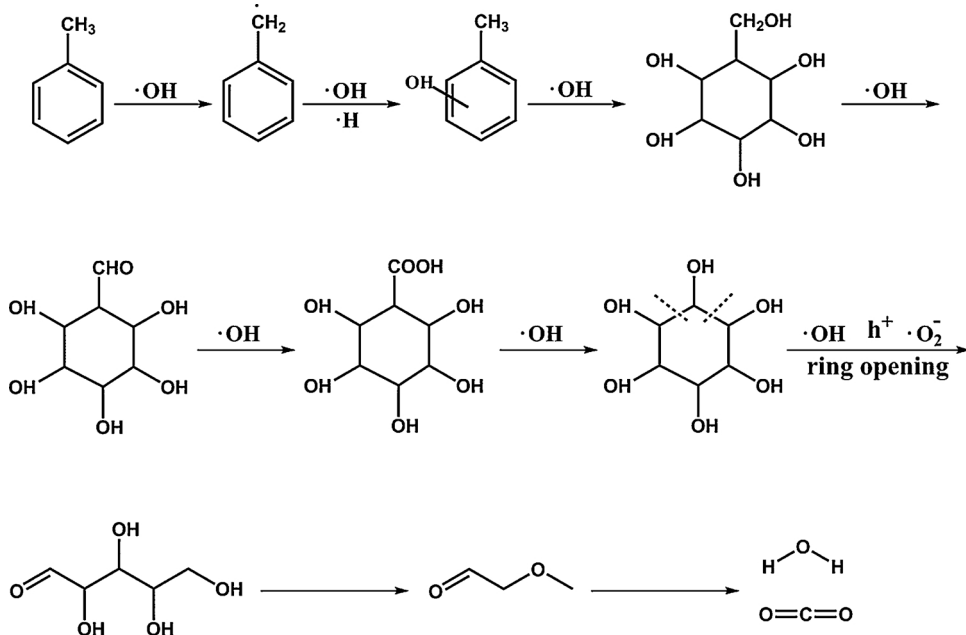


Fig. 8. Proposed pathway of the photocatalytic degradation of toluene over TaON/V₂O₅.

toluene into H₂O and CO₂, are the important indicators to show the ring open of benzene. According to theoretical calculation and fragment ion, toluene was first oxidized by ·OH to generate cyclohexane-1,2,3,4,5,6-hexaol, which subsequently reacted with ·OH, ·O₂⁻ and h⁺ to change into xylose and methoxyacetaldehyde until they were mineralized to CO₂ (Fig. 8). These results may imply that the formation and conversion of xylose and methoxyacetaldehyde is sluggish in kinetics and is the rate-determining step for degradation of toluene.

4. Conclusions

In short, a novel heterojunction photocatalyst of 5 wt% TaON/V₂O₅ was synthesized. This catalyst exhibited excellent photocatalytic activity and could deeply decompose typical VACs, toluene. In addition, it had a wide range of light absorption with good stability for repeated use. Toluene was first oxidized by ·OH to produce cyclohexane-1,2,3,4,5,6-hexaol. Afterwards, it reacted with ·OH, ·O₂⁻ and h⁺ to change into xylose and methoxyacetaldehyde until they were mineralized to CO₂. This work provides a promising strategy for developing highly efficient photocatalysts with wide spectrum absorption for VACs purification.

Acknowledgments

This work was supported primarily by the National Natural Science Foundation of China (51872135, 51572121, 21603098, 21633004, 11504162, and 21876015), the Natural Science Foundation of Jiangsu Province (BK20151265, BK20150580, and BK20161277), the Natural Science Foundation of Jiangsu Education Department (16KJB610002), the Postdoctoral Science Foundation of China (2017M611784) and the Fundamental Research Funds for the Central Universities (021314380133 and 021314380084).

Appendix A. Supplementary data

Supplementary material related to this article can be found, in the online version, at doi:<https://doi.org/10.1016/j.apcatb.2018.12.067>.

References

- [1] T. Ohura, T. Amagai, X. Shen, S. Li, P. Zhang, L. Zhu, *Atmos. Environ.* 43 (2009) 6352–6359.
- [2] S.N. Sarma, Y.J. Kim, J.C. Ryu, *Toxicology* 271 (2010) 122–130.
- [3] H. Guo, S.C. Lee, L.Y. Chan, W.M. Li, *Environ. Res.* 94 (2004) 57–66.
- [4] K. Sexton, J.L. Adgate, G. Ramachandran, G.C. Pratt, S.J. Mongin, T.H. Stock, M.T. Morandi, *Environ. Sci. Technol.* 38 (2004) 423–430.
- [5] K.H. Kim, S.A. Jahan, E. Kabir, R.J.C. Brown, *Environ. Int.* 60 (2013) 71–80.
- [6] P. Thanh-Dong, B.K. Lee, C.H. Lee, *Appl. Catal. B-Environ.* 182 (2016) 172–183.
- [7] P. Thanh-Dong, B.K. Lee, J. Hazard. Mater. 300 (2015) 493–503.
- [8] M. Mao, Y. Li, J. Hou, M. Zeng, X. Zhao, *Appl. Catal. B-Environ.* 174 (2015) 496–503.
- [9] J. Mo, Y. Zhang, Q. Xu, *Appl. Catal. B-Environ.* 132 (2013) 212–218.
- [10] M. Sleiman, P. Conchon, C. Ferronato, J.M. Chovelon, *Appl. Catal. B-Environ.* 86 (2009) 159–165.
- [11] D. Kibanova, J. Cervini-Silva, H. Destaillats, *Environ. Sci. Technol.* 43 (2009) 1500–1506.
- [12] J. Mo, Y. Zhang, Q. Xu, Y. Zhu, J.J. Lamson, R. Zhao, *Appl. Catal. B-Environ.* 89 (2009) 570–576.
- [13] F. Fresno, M.D. Hernandez-Alonso, D. Tudela, J.M. Coronado, J. Soria, *Appl. Catal. B-Environ.* 84 (2008) 598–606.
- [14] B. Liu, X. Li, Q. Zhao, J. Liu, S. Liu, S. Wang, M. Tade, *J. Mater. Chem. A* 3 (2015) 15163–15170.
- [15] Y. Liu, L. Wang, W. Jin, C. Zhang, M. Zhou, W. Chen, *J. Alloys. Compd.* 690 (2017) 604–611.
- [16] P. Avila, A. Bahamonde, J. Blanco, B. Sanchez, A.I. Cardona, M. Romero, *Appl. Catal. B-Environ.* 17 (1998) 75–88.
- [17] C. Zhao, Y. Song, Y. Yang, W. Chen, X. Li, Z. Wang, *Funct. Mater. Lett.* 8 (2015).
- [18] M.C. Nevarez-Martinez, P. Mazierski, M.P. Kobylanski, G. Szczepanska, G. Trykowski, A. Malankowska, M. Kozak, P.J. Espinoza-Montero, A. Zaleska-Medyńska, *Molecules* (Basel, Switzerland) 22 (2017).
- [19] F. Dong, Y. Sun, M. Fu, *Int. J. Photoenergy* (2012).
- [20] Z. Wu, F. Dong, Y. Liu, H. Wang, *Catal. Commun.* 11 (2009) 82–86.
- [21] Y. He, T. Sheng, J. Chen, R. Fu, S. Hu, X. Wu, *Catal. Commun.* 10 (2009) 1354–1357.
- [22] F. Chen, J. Wang, J.Q. Xu, X.P. Zhou, *Appl. Catal. A-Gen.* 348 (2008) 54–59.
- [23] Y.M. He, Y. Wu, H. Guo, T.L. Sheng, X.T. Wu, J. Hazard. Mater. 169 (2009) 855–860.
- [24] J. Sun, X. Li, Q. Zhao, J. Ke, D. Zhang, *J. Phys. Chem. C* 118 (2014) 10113–10121.
- [25] M.Y. Tsang, N.E. Pridmore, L.J. Gillie, Y.H. Chou, R. Brydson, R.E. Douthwaite, *Adv. Mater.* 24 (2012) 3406–3409.
- [26] Y. Chen, S. Liang, L. Wen, W. Wu, R. Yuan, X. Wang, L. Wu, *Phys. Chem. Chem. Phys.* 15 (2013) 12742–12747.
- [27] J. Kou, Z. Li, Y. Yuan, H. Zhang, Y. Wang, Z. Zou, *Environ. Sci. Technol.* 43 (2009) 2919–2924.
- [28] G. Hitoki, T. Takata, J.N. Kondo, M. Hara, H. Kobayashi, K. Domen, *Chem. Commun.* (2002) 1698–1699.
- [29] Z. Wang, J. Hou, C. Yang, S. Jiao, K. Huang, H. Zhu, *Energy Environ. Sci.* 6 (2013) 2134–2144.
- [30] M. Hara, J. Nunoshige, T. Takata, J.N. Kondo, K. Domen, *Chem. Commun.* (2003) 3000–3001.
- [31] Z. Wang, K. Xie, L. Zhao, B. Zhang, *Chem. Commun.* 51 (2015) 2437–2439.
- [32] J. Hou, C. Yang, H. Cheng, S. Jiao, O. Takeda, H. Zhu, *Energy Environ. Sci.* 7 (2014) 3758–3768.
- [33] Y. Zhou, G. Chen, Y. Liu, F. He, *Adv. Mater. Interfaces* 3 (2016).
- [34] N.K. Allam, B.S. Shaheen, A.M. Hafez, *ACS Appl. Mater. Int.* 6 (2014) 4609–4615.
- [35] C.W. Zou, Y.F. Rao, A. Alyamani, W. Chu, M.J. Chen, D.A. Patterson, E.A.C. Emanuelsson, W. Gao, *Langmuir* 26 (2010) 11615–11620.